Research Article

Integrated dopaminergic neuronal model with reduced intracellular processes and inhibitory autoreceptors

Maell Cullen, KongFatt Wong-Lin ✉

Intelligent Systems Research Centre, University of Ulster, Magee Campus, Northland Road, L'Derry BT48 7JL, Northern Ireland, UK
✉ *E-mail: k.wong-lin@ulster.ac.uk*

Abstract: Dopamine (DA) is an important neurotransmitter for multiple brain functions, and dysfunctions of the dopaminergic system are implicated in neurological and neuropsychiatric disorders. Although the dopaminergic system has been studied at multiple levels, an integrated and efficient computational model that bridges from molecular to neuronal circuit level is still lacking. In this study, the authors aim to develop a realistic yet efficient computational model of a dopaminergic pre-synaptic terminal. They first systematically perturb the variables/substrates of an established computational model of DA synthesis, release and uptake, and based on their relative dynamical timescales and steady-state changes, approximate and reduce the model into two versions: one for simulating hourly timescale, and another for millisecond timescale. They show that the original and reduced models exhibit rather similar steady and perturbed states, whereas the reduced models are more computationally efficient and illuminate the underlying key mechanisms. They then incorporate the reduced fast model into a spiking neuronal model that can realistically simulate the spiking behaviour of dopaminergic neurons. In addition, they successfully include autoreceptor-mediated inhibitory current explicitly in the neuronal model. This integrated computational model provides the first step toward an efficient computational platform for realistic multiscale simulation of dopaminergic systems in *in silico* neuropharmacology.

1 Introduction

Dopamine (DA) is a neurotransmitter released by neurons in subcortical brain regions to various other brain regions. The DA system has been extensively studied due to its critical roles in regulating multiple brain functions, which include motor control, motivation, learning, goal-oriented behaviour, hypertension and hormone regulation [1]. In particular a large number of studies have shown the phasic DA activity and prediction error in reinforcement learning [2, 3]. Under or overexpression of DA signalling and other dysfunctions in the mesocorticolimbic DA system have been linked to a number of brain disorders ranging from cognitive deficits to neurodegenerative disorders such as Parkinson's disease, and hence many pharmacologically active compounds that interact with DA system have been developed and used clinically [4–8]. Moreover, drugs such as cocaine, amphetamines and L-3,4-dihydroxyphenylamine (L-DOPA), a DA precursor, can induce psychotic episodes by increasing DA levels [9]. Several features of addiction have been attributed to the DA system such as both short- and long-term changes in the firing of DA neurons in the ventral tegmental area [10] and a significant, long-term down regulation of DA receptors in the striatum [11]. Hence, the DA system is a highly important target in neuropharmacology.

DA acts on multiple receptors, which can be generally divided into D1- and D2-like families [12]. Pre- and post-synaptic D2-like DA autoreceptors are major targets for antipsychotic drugs as they govern several aspects of DA activity including synthesis, release and neuronal activity. The firing rate of dopaminergic neurons is inversely correlated with D2-like autoreceptor activity within the somatodendritic terminal. These receptors respond to an increase in extracellular DA by activating G-protein-coupled-inwardly rectifying potassium channels [13], reducing the excitability of the DA axon terminal and suppressing the firing rate of these neurons [14]. Pre-synaptic autoreceptors also interact with DA release from the axonal terminal and modulate synthesis and release. The binding of DA to autoreceptors at the neuron terminal limits DA synthesis by inhibiting tyrosine hydroxylase (TH), thus decelerating the conversion of tyrosine to L-DOPA [15]. Repeated exposure to psychostimulants that inhibit DA uptake such as cocaine and methamphetamine causes decreased activity of the autoreceptors [16, 17] and the disinhibition of cellular excitability, culminating in an increased likelihood of future substance abuse [18]. Mice without D2 receptors on DA neurons are also hypersensitive to the psychomotor and rewarding effects of cocaine [19].

Indeed, the DA system has been the target of some effective pharmacological treatments for pathological conditions. Indirect DA receptor agonists, together with L-DOPA, have been used to reduce symptom severity of Parkinson's disease patients with great efficacy [20]. Although DA replacement therapy serves only to alleviate symptoms and has not been known to treat Parkinson's disease, it has led to the discovery of more DA receptor agonists, a search that could be improved with the use of computational models. The DA system has also been the target of drugs prescribed for pituitary tumours [21], type 2 diabetes [22], depression and bipolar disorder [23].

Significant progress has been made in discovering the structural, genetic, physiological and pharmacological properties of DA neurons [24]. This has facilitated the development of sufficiently realistic computational models, which include DA synthesis, release and reuptake, and signal transduction [25–27]. Biologically plausible computational models of neuromodulation can assist in furthering our understanding of how neuromodulators contribute at the neuronal circuit and behavioural levels [28–31]. As neuromodulators act across multiple spatial and temporal scales, an important modelling approach is to develop multiscale models, which are unfortunately not yet as prevalent in the pharmaceutical industry as other approaches such as models in genomics, molecular/cellular biology, pharmacokinetics and metabolism [32, 33]. An essential element of multiscale models is to extract relevant and important factors or processes at one scale (e.g.
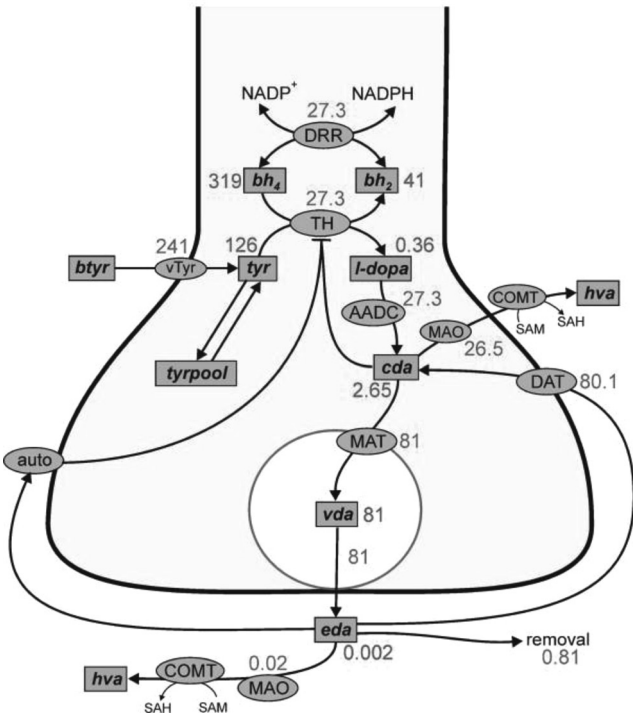
Fig. 1 *Biochemical processes within a dopaminergic pre-synaptic terminal. Numbers denote steady-state concentrations of substrates (red) and fluxes/velocities (blue). Adapted from [26]*

molecular) to bridge and interact with those at other scales [34]. However, it is sometimes not immediately clear which factors or processes are relatively more important for retention. In particular, for the DA pre-synaptic terminal computational model of [26], the relative influences and timescales of the intracellular processes are unclear.

In this paper, we will focus on this established model of pre-synaptic terminal of DA synthesis, release and reuptake [26]. The model can be used to investigate the intracellular effects due to DA concentration level, enzyme expression levels, tyrosine inputs and DA transporters (Fig. 1). However, the model consists of several coupled non-linear differential equations and mathematical functions and variables that may potentially respond with very different timescales and amplitudes. Moreover, the DA neuron is not explicitly modelled in [26]. This poses a significant problem for developing computationally efficient multiscale models of DA system from molecular to neuronal circuit levels.

In this paper, we first analyse the various components of this model [26] by systematically perturbing its variables (substrates) [35]. Results from the perturbation analysis are used to categorise the model variables based on their relative importance and relation to other variables, and also to tease apart the relative timescales of the variables, thus highlighting the key underlying mechanisms and providing the conditions for model reduction. The computational costs of simulating the two reduced (slow and fast) models are compared with that of the original full model. The reduced fast model is then incorporated into a spiking neuronal model with an explicit D2-like autoreceptor-mediated inhibitory current. Finally, this integrated model is used to simulate the effects of pharmacological drugs.

2 Computational model of DA synthesis, release and reuptake

The model in [26] consists of biochemical reactions that occur during the synthesis, release, catabolism and reuptake of DA within the pre-synaptic terminal. A schematic diagram of the model including these reactions is shown in Fig. 1. The model consists of nine coupled non-linear differential equations that describe the chemical kinetics of the various substrates involved in maintaining homeostatic DA synthesis and release (see (1)–(9) and Table 1). The substrates are denoted in lower case while the enzyme names and reaction velocities or rates are denoted in upper case. Transport and reaction velocities are denoted by a capital V followed by the name of the enzyme, transporter or process in subscript. For example, tyrosine hydroxylase, denoted by the symbol TH is the rate limiting enzyme of DA synthesis; autoreceptors exert their inhibitory effect through this mechanism by slowing the conversion of tyrosine to L-DOPA (l-dopa) in the presence of increased firing rates. V_{TH} (tyr, bh4, cda, eda) denotes the velocity (function) of the TH reaction and its dependence on the concentrations of the substrates tyrosine (tyr), tetrahydrobiopterin (bh4), cytosolic DA (cda) and extracellular DA (eda).

$$\frac{d[bh2]}{dt} = V_{TH}(\text{tyr, bh4, cda, eda}) \\ - V_{DRR}(\text{bh2, NADPH, bh4, NADP}) \quad (1)$$

$$\frac{d[bh4]}{dt} = V_{DRR}(\text{bh2, NADPH, bh4, NADP}) \\ - V_{TH}(\text{tyr, bh4, cda, eda}) \quad (2)$$

$$\frac{d[tyr]}{dt} = V_{TYRin}(\text{btyr}(t)) - V_{TH}(\text{tyr, bh4, cda, eda}) - k_1 \\ \times [\text{tyr}] + k_{-1} \times [\text{tyrpool}] - k_{tyr}^{catab} \times [\text{tyr}] \quad (3)$$

Table 1 Steady-state values for the substrates and velocities in the model

Substrate/rate	Full name	Steady-state value			
		Fast model	Slow model	Full model	[26]
[bh2]	dihydrobiopterin	37	41.9	22.7	41
[bh4]	tetrahydrobiopterin	327.2	322	337.2	319
[l-dopa]	3,4-dihyroxyphenylalanine	0.37	0.35	0.34	0.36
[tyr]	tyrosine	142	103.6	93.4	126
[tyr-pool]	tyrosine pool	1068	777	701	not given
[hva]	homovanillic acid	5.9	8.3	6.26	not given
[cda]	cystosolic DA	1.6	2.8	4.2	2.65
[vda]	vesicular DA	80.7	77.8	78	81
[eda]	extracellular DA	0.013	0.012	0.012	0.002
V_{TH}	tyrosine hydroxylase	28.4	27.2	26.7	27.3
V_{DRR}	dihydropteridine reductase	24.9	27.2	26.7	27.3
V_{tyrin}	neutral amino acid transporter	241	241	241	241
V_{AADC}	aromatic amino acid decarboxylase	26	26.1	26.7	27.3
V_{MAT}	vesicular monoamine transporter	80.7	65.6	77.5	81
V_{DAT}	DA (reuptake) transporter	75	68	72.3	80.1
V_{catab}	catabolism of extracellular DA	0.3	0.13	0.12	0.02

$$\frac{d[l-dopa]}{dt} = V_{TH}(tyr,\ bh4,\ cda,\ eda) - V_{AADC}(l-dopa) \quad (4)$$

$$\frac{d[cda]}{dt} = V_{AADC}(l-dopa) - V_{MAT}(cda,\ vda) + V_{DAT}(eda)$$
$$- k_{cda}^{catab} \times cda \quad (5)$$

$$\frac{d(vda)}{dt} = V_{MAT}(cda,\ vda) - fire(t) \times vda \quad (6)$$

$$\frac{d(eda)}{dt} = fire(t) \times vda - V_{DAT}(eda) - V_{CATAB}(eda) - k_{rem}$$
$$\times eda \quad (7)$$

$$\frac{d(hva)}{dt} = k_{cda}^{catab} \times cda + V_{CATAB}(eda) - k_{hva}^{catab} \times hva \quad (8)$$

$$\frac{d(tyrpool)}{dt} = k_1 \times tyr - k_{-1} \times tyrpool - k_{tyrpool}^{catab} \times tyrpool \quad (9)$$

The function $fire(t)$ in (6) and (7) relates to the firing rate of the (pre-synaptic) DA neurons and is generally time dependent [26]. In this paper, we initially follow [26] and set the value to be 1 micromole per hour (μM/h), that is, vesicular DA is released at a constant rate with entire pool turning over every hour. When we later incorporate a spiking neuronal model, this function becomes an instantaneous step function (delta function) whenever a DA neuronal spike occurs. The specific functional forms of the reaction velocities used for (1)–(9) are determined by Michaelis–Menten kinetics as follows [26]:

$$V_{TH}(tyr,\ bh4,\ eda,\ cda)$$
$$= \left(\frac{0.56}{1 + ([tyr]/K_{i(tyr)})} \right) \times \left(\frac{4.5}{(8([eda]/0.002024)^4 + 1)} + 0.5 \right)$$
$$\times \left(\frac{V_{max} \times [tyr] \times [bh4]}{[tyr][bh4] + K_{tyr}[bh4] + K_{tyr}K_{bh4}(1 + ([cda]/K_{i(cda)}))} \right) \quad (10)$$

$$V_{tyrin}(btyr) = \frac{400[btyr]}{64 + [btyr]} \quad (11)$$

(see (12))

$$V_{AADC}(l-dopa) = \frac{V_{AADC,max} \times [l-dopa]}{k_{AADC,m} + [l-dopa]} \quad (13)$$

$$V_{MAT}(cda,\ vda) = \frac{V_{MAT,max} \times [cda]}{k_{MAT,m} + [cda]} - k_{out} \times [vda] \quad (14)$$

$$V_{DAT}(eda) = \frac{V_{DAT,max} \times [eda]}{k_{DAT,m} + [eda]} \quad (15)$$

$$V_{catab}(eda) = \frac{V_{catab,max} \times [eda]}{k_{catab,m} + [eda]} \quad (16)$$

The kinetic parameters (with units in μM, μM/h) are taken from [19] with the exception of those denoted by a * which are from [34]: $k_{AADC,m} = 130$, $V_{AADC,max} = 10,000$, $k_{DAT,m} = 1.4$, $V_{DAT,max} = 8000$, $k_m^{bh2} = 100$, $V_{DRR,max}^f = 150$, $k_m^{bh4} = 10$, $k_m^{NADP} = 75$, $k_m^{NADPH} = 75$, $V_{max}^b = 120$, $k_{MAT,m} = 0.55$, $V_{MAT,max} = 7082$, $k_{out} = 80$, $K_{tyr} = 130$, $K_{bh4} = 60$, $V_{max} = 120$, $K_{i(cda)} = 110$, $K_{i(tyr)} = 160$, nicotinamide adenine dinucleotide phosphate (NADPH) = 124*, NADP = 0.25*,

$k_1 = 6$, $k_{-1} = 0.6$, $k_{tyr-pool}^{catab} = 0.2$, $k_{tyr}^{catab} = 0.8$, $k_{cda}^{catab} = 5$, $k_{catab,m} = 3$, $V_{catab,max} = 30$, $k_{hva}^{catab} = 3.45$ and $k_{rem} = 400$.

The initial values for NADPH and 2-oxoaldehyde dehydrogenase (NADP+) are not readily provided in [19] and are obtained from [35], taken as 124 and 0.25 μM, respectively. The ratio of NADPH to NADP+ is described as 500:1 [36], consistent with those used in this model. The final steady-state values are consistent with those in [26] (Table 1).

The full model is simulated in MATLAB (MATLAB R2013b, The MathWorks, Natick, MA) with Euler's numerical scheme being used for integrating the differential equations. The time step size used for numerical integration in the model is 0.00001 h (0.0036 s). MATLAB codes are provided in Appendix 2.

3 Results

Intrinsically fast and slow dependent variables or substrates were elucidated by carrying out step perturbation of each variable and substrate while analysing the state of the full model at each step. This 'separation of timescales' approach can allow the model to be reduced for increased computational speed allowing the user to investigate either slow or fast dynamics independently with greater efficacy [35]. For example, if fast timescale is the focus of study (e.g. order of milliseconds), the much slower variables (e.g. ~hours) can be assumed to be relatively constant, and are converted from differential equations to mere mathematical functions or constants. The model is then reduced to a 'fast mode' with reduced computational cost. Similarly, if a slow timescale is the focus (e.g. order of hours), the much faster variables (e.g. ~milliseconds) are assumed to have rapidly reached their quasi-steady states, that is, they become mathematical functions. Again, we can achieve faster computational speed. Therefore, in principle, we can have two approximate yet efficient computational models; one that can be used to simulate and examine fast dynamics, and the other for slower dynamics. Further model reduction can be achieved by observing the relative magnitude of how change in one substrate can affect another substrate. For example, if the perturbation of substrate A elicits a relatively small change in the concentration of substrate B, then the dynamical A-to-B relationship can be ignored (see Section 3.2). To search for the relative timescales and magnitude changes of one substrate over another, we resort to perturbation of the variables as discussed below.

3.1 Model perturbation and categorisation

Before onset of perturbation, the system is first simulated and allowed to reach its steady states. Then perturbation for each substrate/variable (e.g. tyr) is carried out by abruptly changing one of the contingent substrates/variables (e.g. bh4, cda or eda) in a step-wise manner (Fig. 2) [35]. The system is then allowed to reach its new steady state during the perturbed phase. We have also tried alternative perturbation methods – by perturbing the system's stimuli/inputs, and observing the global effects. However, the results do not provide a level of acuity nor consistency to distinguish the substrates' timescales and substrate-to-substrate coupling strengths. The resultant reduced models also do not replicate the behaviour of the original full model well.

Assuming a substrate increases exponentially toward its new steady state following perturbation, we find the amount of time (τ) it takes for the dependent variable to reach 67% (33% in cases of exponential decay) of the new steady state (Fig. 2). If τ for that particular variable is relatively fast, the relative variable or substrate is categorised as a fast variable. Similarly if τ is slow, the variable/substrate is categorised as slow. Specifically,

$$V_{DRR}(bh2,\ NADPH,\ bh4,\ NADP) = \left(\frac{V_{max}^f \times [bh2] \times NADPH}{(k_m^{bh2} + [bh2])(k_m^{NADPH} + NADPH)} \right) - \left(\frac{V_{max}^b \times [bh4] \times NADP}{(k_m^{bh4} + [bh4])(k_m^{NADP} + NADP)} \right) \quad (12)$$
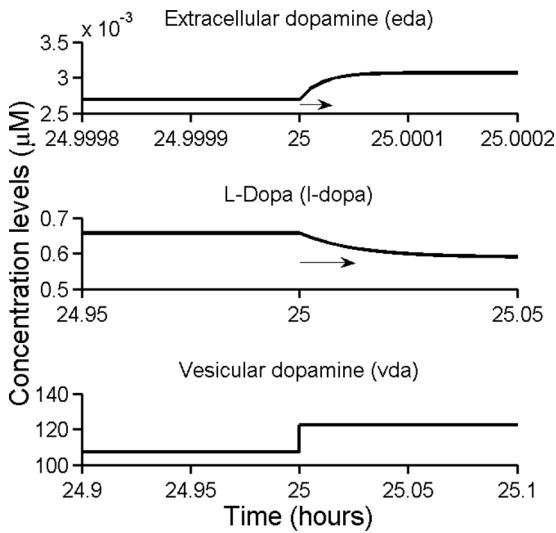
Fig. 2 *Example of responses of the variables/substrates (extracellular DA (eda) and L-DOPA (l-dopa)) over time during a step perturbation of another variable/substrate (vesicular DA, vda). Arrows denote the evaluated timescales of eda and l-dopa. Note the different scales on the horizontal and vertical axes. Perturbation occurs from the 25th hour onwards*

under this range of perturbation levels, we calculate the mean of time constants. Substrates with mean time constants <0.05 will be labelled as fast, whereas those >0.20 as slow. In between these two values, substrates will be classified as intermediate. There will also be substrates with relatively larger standard deviation in the time constants. Hence, if the standard deviation is >0.05 and comparable with their mean value, we will assume the substrate to be classified as mixed. For example, cda has a mean of 0.056 and standard deviation of 0.062. Therefore, it will be classified as a substrate with intermediate or mixed timescales. This process is repeated for other substrates/variables with different perturbing amplitudes (1.5, 2 and 3 times the respective steady-state or baseline value), and the overall results are presented in Table 2, which shows all the variables/substrates dynamics as having intrinsically slow, fast or intermediate/mixed dynamics, and then categorised based on the classification criteria. Clearly, the timescales can vary greatly from one substrate to another. For example, in terms of

timescales, [cda] responds to perturbation of [vda] with about two orders of magnitude faster than [l-dopa] responding to the same [vda] perturbation.

Similarly, Table 3 (top) shows the relative (percentage) changes in steady-state values from baseline values for the perturbation of all variables/substrates, whereas the bottom reveals their coupling strengths based on the classification criteria of the (absolute) mean and standard deviation of the percentage change. Specifically, if the mean of the coupling strength's percentage change is <3, the coupling will be classified as weak, whereas if >35, it will be classified as strong. Couplings will be classified under the intermediate category if the values lie between these two values, and mixed if the standard deviations are >20 and comparable with their mean values. The percentage change in steady states can vary widely, similar to the wide range of the timescales. For example, [bh2] is much more dependent on [cda] and [eda] than [bh4] and [tyr].

3.2 Reduced slow model

To obtain a reduced slow model, fast substrates will be assumed to have rapidly reached their steady states and their associated differential equations will be transformed into functions, that is, at their steady-state values. For example, we can set the differential (7) for the fast substrate eda, $d[eda]/dt = 0$, and solve the resultant algebraic equation (using the Mathematica software package) [35], we can obtain

$$[eda] = \frac{\text{fire}(t) \times \text{release} \times k_m^{\text{catab,eda}} \cdot \text{vda} \cdot k_{\text{DAT},m}}{\left(k_{\text{rem}} \times k_m^{\text{catab,eda}} + V_{\max}^{\text{catab,eda}}\right) \times k_{\text{DAT},m} + k_m^{\text{catab,eda}} \times V_{\text{DAT,max}}} \quad (17)$$

Similarly for the other fast variables vda and hva. If we instead wish to obtain a reduced fast model, then the slow substrates can be set to be assumed to be approximately constant (with specific steady-state values initially obtained from the full model simulations), and similar solving of the algebraic equations will be required. Specifically, we could keep the dynamics of the fast variables eda, vda and hva, and set the rest of slow and intermediate/mixed variables to be constant. For example, if we have set $d[l\text{-dopa}]/dt = 0$ in (4), we would have obtained

$$[l - \text{dopa}] = \frac{V_{\text{TH}}(\text{tyr, bh4, cda, eda}) \times k_{\text{AADC},m}}{V_{\text{AADC,max}} - V_{\text{TH}}(\text{tyr, bh4, cda, eda})} \quad (18)$$

Table 2 Top: Rise and decay time constants (τ) (in 10^{-5} h) of substrates/variables after perturbations. Bottom: Classification of substrates/variables' timescales

Substrate	Perturbed	Perturbation, %			Mean	Standard deviation	Class
		150	200	300			
bh2	tyr	0.097	0.096396	0.094077	0.195	0.0975	mixed
bh2	bh4	0.332531	0.324372	0.325767			
bh2	cda	0.182653	0.178864	0.176167			
bh2	eda	0.17579	0.17278	0.17171			
bh4	bh2	1.78121	8.197055	12.66077	2.016	4.084	slow
bh4	tyr	0.058466	0.063716	0.64047			
bh4	cda	0.129081	0.127165	0.126272			
bh4	eda	0.125855	0.12221	0.12308			
l-dopa	tyr	0.09912	0.099502	0.099872	0.083	0.022	mixed
l-dopa	bh4	0.088901	0.090077	0.092284			
l-dopa	cda	0.064116	0.078224	0.081265			
l-dopa	vda	0.038861	0.050756	0.114403			
cda	l-dopa	0.14398	0.125	0.102	0.056	0.062	mixed
cda	vda	0.000323	0.001769	0.009089			
cda	eda	0.064515	0.16417	0.05702			
vda	cda	0.002426	0.002426	0.002429	0.002	0	fast
eda	vda	0.059719	0.051678	0.037623	0.05	0.011	fast
hva	cda	0.028875	0.028845	0.028832	0.029	0	fast
tyr-pool	tyr	0.124305	0.124	0.125	0.124	0	slow
tyr	tyr-pool	0.012233	0.0119	0.021202	0.535	0.32	slow
tyr	bh4	0.62187	0.60798	0.60286			
tyr	cda	0.757081	0.753788	0.757526			
tyr	eda	0.75229	0.75692	0.768391			

Table 3 Top: Percentage change in steady states of substrates/variables after perturbation. Bottom: Classification of substrates/variables' coupling strengths

Substrate	Perturbed	Perturbation, %			Mean	Standard deviation	Class
		150	200	300			
bh2	tyr	4	6.4	14.47	8.29	5.48	intermediate
bh2	bh4	0.64	1.01	1.37	1	0.37	weak
bh2	cda	−28.75	−37.55	−43.77	−36.7	7.55	strong
bh2	eda	−41.58	−49.33	−52.33	−47.75	5.55	strong
bh4	bh2	30.62	44.81	74.8	50.08	22.56	strong
bh4	tyr	4.61	7.07	10.05	7.24	2.72	intermediate
bh4	cda	−0.86	−2.79	−3.4	−2.35	1.33	weak
bh4	eda	2.45	5.34	6.85	4.88	2.24	intermediate
l-dopa	tyr	12.02	17.09	22.2	17.1	5.09	intermediate
l-dopa	bh4	1.82	2.63	3.38	2.61	0.78	weak
l-dopa	cda	2.7	7.89	11.06	7.22	4.22	intermediate
l-dopa	vda	−9.47	−9.42	−32.91	−17.27	13.55	mixed
cda	l-dopa	72.98	17.89	39.34	43.4	27.77	strong
cda	vda	−30.76	−83.14	−99.8	−71.23	36.03	strong
cda	eda	11.14	23	58.48	30.87	24.63	mixed
vda	cda	7.67	3.0755	17.19	9.31	7.2	intermediate
eda	vda	12.29	34.06	56.19	34.18	21.95	mixed
hva	cda	3.02	8.02	14.81	8.62	5.92	intermediate
tyr-pool	tyr	55.24	67.39	70.16	64.26	7.94	strong
tyr	tyr-pool	70.17	80.93	70.172	73.76	6.21	strong
tyr	bh4	−43.68	−80.94	−235.38	−120	101.64	mixed
tyr	cda	63.15	62.54	62.03	62.57	0.56	strong
tyr	eda	37.78	38.43	48.67	41.63	6.11	strong

and similarly for other slow variables. See Appendix 1 for details. From our simulations, we find that the steady states of the full and reduced model are reasonably well matched, while all kinetic parameters remain within the ranges presented in the literature (see Table 1).

In Fig. 3, we can see the steady states of the full and reduced slow models (see Table 1) have similar values. On perturbing the blood
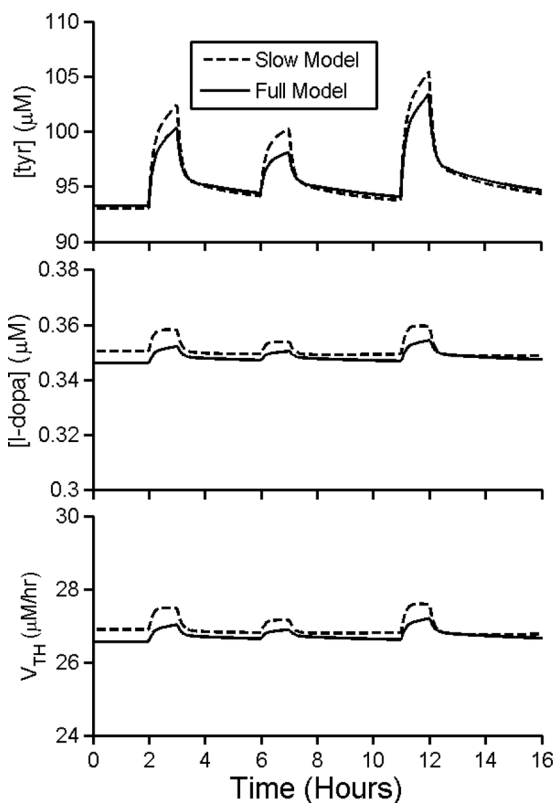
Fig. 3 *Comparison of full and reduced slow model under perturbation. The blood tyrosine concentration [btyr] is altered (using a step function) over time to represent three sessions of food intake (meals) and the effects on other fast substrates (vesicular DA (vda) and L-DOPA (l-dopa)) and the velocity of the tyrosine hydroxylase (TH) reaction, V_{TH}, over a 16 h period*

tyrosine (btyr) three times over a 16 h period, simulating the effect of food intake in the form of three meals throughout the waking day, we found that the full and reduced slow model show very similar perturbed behaviours.

Further reduction of the slow model can be achieved by observing the relative effect of one substrate over another. For example, [cda] has relatively smaller effect on [bh4] (Table 3), and we can ignore this factor in the model reduction process.

The execution time for a 48 h simulation of the reduced slow model and the full model are compared using MATLAB's stopwatch timer. By comparing the computational speed of a single run, we found that the reduced slow model with fewer differential equations took 61.32 s to run while the full model took 64.95 s. The simulation times were calculated based on the most computationally intensive part of the code, namely, the numerical integration. If we repeat the simulations over 10,000 runs for 48 h simulation (e.g. in search for optimal drug dosage), then we can save about 10 h of computational time.

3.3 Reduced fast model integrated into a spiking neuron model

Reactions that occur on the scale of milliseconds to tens of seconds are isolated and analysed by either holding substrates with slower dynamics at a constant value or calculating their values as functions at each time step. Homovanillic acid (hva) serves as an endpoint for the catabolism of cytosolic DA (cda) and exhibits fast dynamics. As this model does not explicitly simulate the catabolism of cda, no other substrates are dependent on hva, and therefore it can be excluded from the analysis. The fast model can thus be reduced further by simulating the dynamics of only eda and vda (extracellular and vesicular DAs) with two differential equations and the control parameter for neuronal spiking, 'fire'.

The constant values for the 'slow' substrates can be obtained by simulating either the full or reduced slow model until the difference between the values of substrate X at time T, $X(T)$, and $X(T−1)$ is less than some value ε, where ε is small enough to represent no significant change. In our simulations, we select ε to be 0.002. We found that the reduced fast model with much lesser differential equations was able to complete a 48 h simulation in 61.6 s, 3.35 s faster than the original full model. If the simulation were to be repeated 10,000 times we would save 9.3 h.

To artificially implement the effects of neuronal spiking, the function 'fire' in (6) and (7) will attain an instantaneous value

increase whenever the presumed neuron fires an action potential. On artificially mimicking action potentials or neuronal spiking as in [19], we found that the behaviours of the perturbed substrates in the reduced fast model are similar to that as in the full model (Fig. 4). In particular, not only are the slow substrates or velocities similar, but so are the faster substrates or velocities, for example, vda and eda. Note that vda and eda are both directly influenced by neuronal spiking – the release of DA into the extracellular space involves the reduction of vda and enhancement of eda.
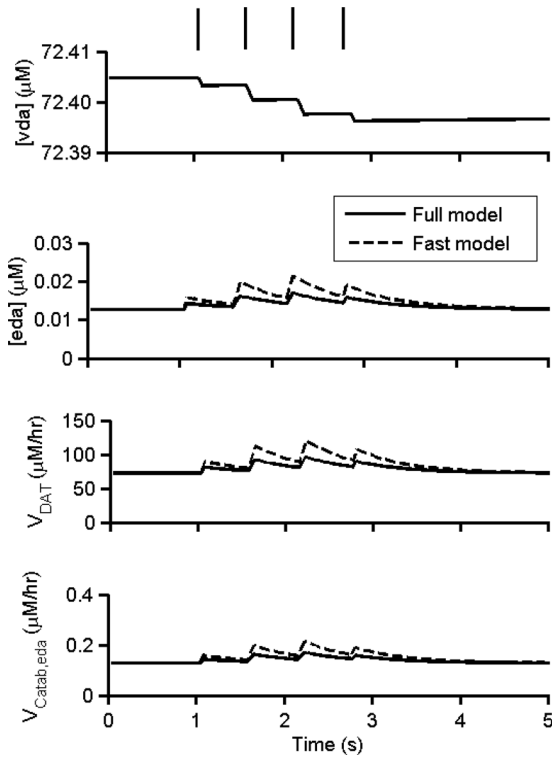
So far, as in [19], the neuron is not explicitly modelled. Here, we improve the model by incorporating a spiking neuronal model with intrinsic bursting behaviour similar to that of experimentally observed dopaminergic neurons [37, 38]. We will make use of the simplified, computationally efficient and highly scalable Izhikevich model, an adaptive quadratic integrate-and-fire neuronal model capable of generating a wide range of biologically plausible neuronal spiking patterns [39]. The membrane potential V of this neuronal model can be described by the differential equation

$$\frac{\mathrm{d}V}{\mathrm{d}t} = 0.04V^2 + 5V + 140 - W + I \quad (19)$$

where I is the overall afferent or input current and W is some recovery variable described by

$$\frac{\mathrm{d}W}{\mathrm{d}t} = a(bV - W) \quad (20)$$

where a and b are parameters that govern the overall timescale of the recovery and the coupling strength, respectively. These two coupled equations describe the membrane dynamics of the neuron, with an after-spike resetting condition: if $V \geq 0$ mV, then V is replaced by c while W by $W + d$, where c and d are model parameters. Hence, the spiking pattern of the Izhikevich model can be controlled

using only these four parameters, a, b, c and d. To capture the general (intrinsically bursting) spiking behaviour as in experiments [37, 38], we set $a = 0.0025(1/ms)$, $b = 0.2(1/mV)$, $c = -55$ mV and $d = 2$.
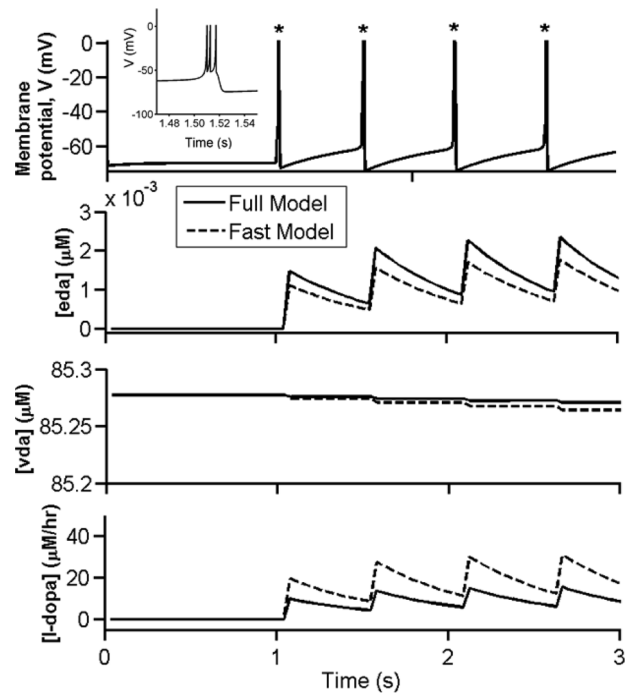
Fig. 5 illustrates this intrinsic bursting at around about 2–3 spikes per burst within ~20 ms duration (Fig. 5, inset), and an interval of ~0.5–1 s between consecutive bursts (Fig. 5, top panel) [37, 38]. Extracellular DA level [eda] varies ~0.01–1 µM during bursting or stimulation, consistent with [40, 41]. To be even more realistic, we set the function 'fire' in (6) and (7) to be zero when the neuron is not spiking, similar to that in [35]. The simulation in Fig. 5 shows that the substrates do not vary greatly between the reduced fast model and the full model. Note that the activities have now been changed. For example, the initial [eda] before neuronal firing is at zero. This is justifiable given that in a more natural condition there will be multiple active dopaminergic neurons contributing to the increased baseline [eda] concentration observable *in vivo*.

### 3.4 Inhibitory autoreceptors

It has been known that dopaminergic autoreceptors can not only affect DA synthesis and release [26, 42], but also inhibit neuronal excitability. As previous models of dopaminergic pre-synaptic terminal did not include such a specific autoinhibitory current-based mechanism, we make use of our reduced fast neuronal model to further explore such combined effects. We validated the incorporation of the autoreceptors to our model against the results recorded from electrophysiological and computational studies as shown below.

Our reduced pre-synaptic terminal dopaminergic neuronal model is completed by incorporating additional inhibitory currents into the Izhikevich model [39]. Specifically, the additional current depends on [eda] as follows:

$$I_{\text{auto}} = -\frac{f}{1 + e^{-g([eda]-h)}} \quad (21)$$

Fig. 4 *Example of responses of the variables/rates (vda, eda, V_{DAT} and the catabolism of eda, $V_{catab,eda}$) during a series of artificial spike perturbations (denoted by vertical lines at the top). Note the rate of eda catabolism increases and the concentration of the vda 'reservoir' decreases slightly as eda concentration increases at the time of each spike. Note that [vda] of the full and fast models overlapped*

Fig. 5 *Neuronal bursting activity effects on [eda] and intracellular substrates. Note that each instantaneous change in activities is due to a burst of neuronal membrane potential or spikes (denoted by an asterisk); each burst consists of three spikes (see inset)*
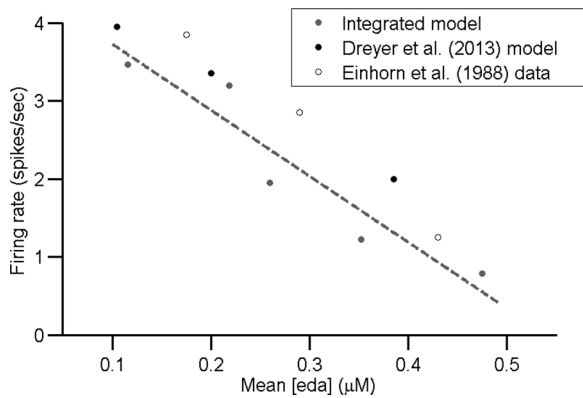
Fig. 6 *Relationship between neuronal firing rate and mean [eda]. Black filled circles: from [43]; grey filled circles: our reduced integrated model; unfilled circles: [45]. In our model, mean [eda] is calculated from averaging the fluctuations (due to neuronal spiking activity) over time. Both firing rate and mean [eda] are evaluated at steady state. Dashed line: fitted only to grey simulated data*

where f, g and h control the overall amplitude, gain or slope, and the offset of the assumed sigmoidal function of the current. Note that for simplicity, we did not include an additional timescale for I_{auto} as observed in [42], although this can be easily achieved by having an additional differential equation for the dynamics of I_{auto}. The values of these parameters are determined by fitting the [eda] and baseline (tonic) neuronal firing rate to experimental data. In [43–45], the coupling between the (somatodendritic) DA levels and neuronal firing rate were determined as a function of cocaine dose, an effective measure of uptake inhibition. Our model is able to exhibit such an inverse linear relationship (Fig. 6).

Since the neuronal model is already intrinsically bursting, we could now investigate how the duration of the burst affects the amount of [eda]. In Fig. 7, we increase the external input current with a step-change in amplitude from 4.55 to 15 to mimic the bursting neuronal activity from tonic firing activity. There is a

phasic increase in [eda], and this increase depends on the duration of the bursting behaviour. Conversely, when the external input current is reduced to 0, mimicking a 'pause' of DA neuronal firing [eda] is reduced. These results look comparable with those in [43].

Next, as in [26], we block the autoreceptors, for example, mimicking the administration of D2-receptor agonists, to understand how the [eda]-versus-firing rate relationship is affected. Best *et al.* [26] have shown that autoreceptors act as a homeostatic mechanism on DA neuronal firing rate by reducing its firing rate range (Fig. 9B in [26]). However, the model presented in [26] does not have an explicit DA autoreceptor-mediated inhibitory current. In the absence of this inhibitory current our integrated model's [eda]-versus-firing rate relationship is similar to that in [26], but a dramatic change is observed when the autoreceptor-mediated inhibitory current is explicitly modelled, shown in Fig. 8 (left panel). In fact, the slope of the curve in the presence of autoreceptors is negative while that in [26] is positive.

Conceptually, DA autoreceptors can provide negative feedback to the intracellular processing [26]. For example, if there is too much [eda], then the autoreceptors will inhibit V_{TH} and reduce the production of [l-dopa], which will subsequently lead to a reduction in [eda]. Conversely, when there is too much [eda], the autoreceptor-induced inhibition on V_{TH} will be reduced and allow more [l-dopa] and [eda] to be subsequently manufactured. It is not clear how autoreceptor-mediated inhibitory current in neurons can influence this dynamic homeostatic process. In Fig. 8 (right), we show that in the absence of this current, [eda] increases almost linearly with increasing [l-dopa] as discussed above. In the presence of the autoreceptor-mediated current, this linear relationship is shifted vertically downwards. This can be explained by realising that the inhibitory current will lead to reduction of neuronal firing rate which and hence lesser [eda]. In other words, for the same amount of [eda] released, there will be more [l-dopa] produced when the autoreceptor-mediated inhibitory current is present. In summary, we have developed a more realistic model of the DA pre-synaptic terminal which explicitly has DA D2 autoreceptors to not only inhibit the intracellular dynamics (via V_{TH}), as in [26], but also simultaneously inhibit the membrane potential of the dopaminergic neuron.
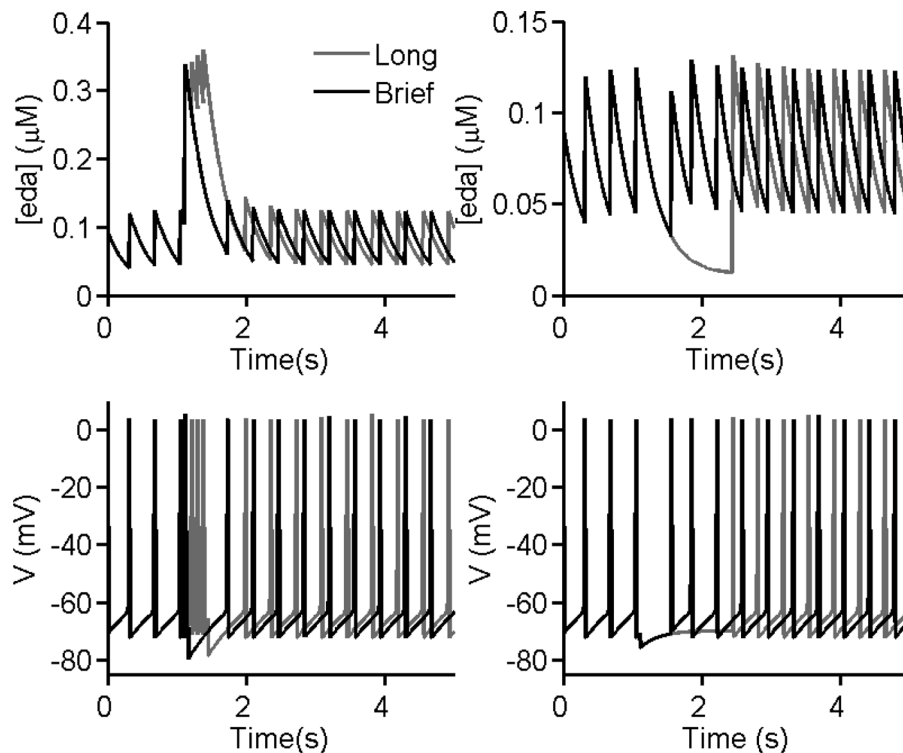
Fig. 7 *Burst and pause on phasic [eda]. Top: [eda]; bottom: neuronal membrane potential. Left: burst; right: pause. Left, black – burst duration of 0.1 s; grey – 0.6 s. Right: black – pause duration of 0.8 s; grey – 2.4 s. Compared with [43]*
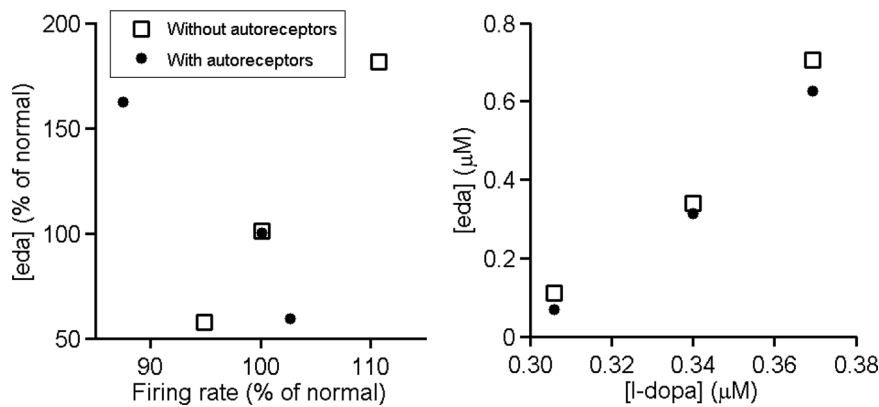
Fig. 8 *Effects of autoreceptor-mediated inhibitory current on homeostatic processes. Left: [eda] versus neuronal firing rate (percentage change from baselines) with and without autoreceptors. The results with autoreceptors are very different from that of [26]. Right: [eda] versus [l-dopa] (absolute values) with and without autoreceptors*

4   Discussion

We have analysed an established computational model of DA synthesis, release and reuptake using a simple perturbation method. This method has previously been successfully applied to a serotonergic pre-synaptic terminal model [35]. In this paper, we have shown similar success for the dopaminergic pre-synaptic terminal model, but with a different set of substrates and reactions. Specifically, we show that different variables or substrates are affected (or perturbed) much more than others. Importantly, the intrinsic timescales of the variables or substrates can vary widely, ranging across several orders of magnitude. This wide range of inherent timescales allows us to separate the slow and fast variables/substrates that subsequently approximate and reduce the original model into a slow and fast version. We found that the reduced slow and fast models are not only more computationally efficient due to the reduced number of differential equations to be numerically integrated, but can also capture same the tonic and phasic activity features as in the full model. Importantly, the simpler model helps to identify the key reactions for a specific timescale.

Next, we incorporate the reduced fast model into a (Izhikevich) spiking neuronal model that can replicate realistic tonic and phasic (bursting) spiking behaviours. This integrated reduced fast model behaves similarly to an integrated model with the full set of intracellular processes. By adding an explicit inhibitory autoreceptor-mediated current into this spiking neuronal model, we show that the model can exhibit suppression of firing rate with increasing [eda] in a linear way, as found in experiments and other computational modelling works [43, 44]. It should be noted that, unlike the model in [43], our model has an explicit neuronal model for the autoreceptor-mediated current to directly inhibit the neuronal membrane excitability. Our integrated model's results also differ from that of the work in [26], which has no autoreceptor-induced inhibition on neuronal firing rate. However, with a more integrated model, it is not immediately clear how large a role (D2-like) autoreceptors can play in terms of the homeostasis of DA neuronal activity, and this deserves further investigation. Overall, our integrated DA pre-synaptic terminal model is not only computationally efficient, but can also explicitly account for key mechanisms during steady states.

In addition to tonic steady states, an important function of DA is its phasic activity behaviour, which is related to behavioural (reinforcement) learning. The high transient extracellular DA level release during DA neuronal bursting has been suggested as a signal that facilitates prediction error and the enforcement of synaptic plasticity within targeted brain regions, which can result in behavioural change [46, 47]. In this paper, we have demonstrated the possibility of large amount of [eda] release following a burst of neuronal spiking from regular spiking at baseline. We have also shown how pause behaviour can quickly reduce the [eda] level. Although correlated with the surprise

absence of an expected reward [46], the actual function of pause activity on behavioural change remains unknown.

Reduced models of neuromodulators can be incorporated into large-scale computational models [28–31, 48–50]. The seemingly small increase in simulation speed will be amplified when we increase the complexity of the model, for example, when simulating multiple neurons simultaneously. In particular, our similar reduced fast model for the serotonergic pre-synaptic terminal has been shown to be successfully implemented in spiking neuronal network models to efficiently simulate an entire population of ∼100,000 serotonergic neurons [35]. We would expect our current integrated model to simulate as efficiently (there are also about a total of ∼100,000 dopaminergic neurons [51]). These reduced models will be useful tools for *in silico* investigations attempting to bridge between molecular, cellular, cognitive and behavioural mechanisms [28–30]. The ability of these models to directly mimic the effects of drugs and genetic polymorphisms [26] will also make them useful for rapid testing in drug discovery and development in neuropharmacology. Further extension of the current work will include modelling the DA post-synaptic effects such as signal transduction and neuronal circuit dynamics at the microcircuit level [48] or at a larger scale [30].

6   References

1   Missale, C., Nash, S.R., Robinson, *et al.*: 'Dopamine receptors: from structure to function', *Physiol. Rev.*, 1998, **78**, pp. 189–225
2   Glimcher, P.W.: 'Understanding dopamine and reinforcement learning: the dopamine reward prediction error hypothesis', *Proc. Natl. Acad. Sci.*, 2011, **108**, pp. 15647–15654
3   Steinberg, E.E., Keiflin, R., Boivin, J.R., *et al.*: 'A causal link between prediction errors, dopamine neurons and learning', *Nat. Neurosci.*, 2013, **16**, pp. 966–973
4   Baldessarini, R.J., Tarazi, F.I.: 'Drugs and the treatment of psychiatric disorders', in Hardman, J.G., Limbird, L.E. (EDs.): 'The pharmacologic basis of therapeutics' (McGraw-Hill, New York, 2001), pp. 485–520
5   Goetz, C.G.: 'Dopaminergic agonists in the treatment of Parkinson's disease', *Neurology*, 1990, **40**, pp. 50–54
6   Damier, P., Hirsch, E.C., Agid, Y., *et al.*: 'The substantia nigra of the human brain II. Patterns of loss of dopamine-containing neurons in Parkinson's disease', *Brain*, 1999, **122**, pp. 1437–1448
7   Laruelle, M., Abi-Dargham, A., Gil, R., *et al.*: 'Increased dopamine transmission in schizophrenia: relationship to illness phases', *Biol. Psychiatry*, 1999, **46**, pp. 56–72
8   El Mansari, M., Guiard, B.P., Chernoloz, O., *et al.*: 'Relevance of norepinephrine–dopamine interactions in the treatment of major depressive disorder', *CNS*

Neurosci. Therapeutics, 2010, **16**, (3), pp. e1–17, doi: 10.1111/j.1755-5949.2010.00146.x

9 Tost, H., Alam, T., Meyer-Lindenberg, A.: 'Dopamine and psychosis: theory, pathomechanisms and intermediate phenotypes', *Neurosci. Biobeh. Rev.*, 2010, **34**, pp. 689–700

10 Bonci, A., Bernardi, G., Grillner, P., *et al.*: 'The dopamine-containing neuron: maestro or simple musician in the orchestra of addiction', *Trends Pharmacol. Sci.*, 2003, **24**, pp. 172–177

11 Volkow, N.D., Fowler, J.S., Wang, G.J., *et al.*: 'Imaging dopamine's role in drug abuse and addiction', *Neuropharmacology*, 2009, **56**, Suppl 1, pp. 3–8

12 Neve, K.A., Seamans, J.K., Trantham-Davidson, H.: 'Dopamine receptor signaling', *J. Receptors Signal Transduct. Res.*, 2004, **24**, pp. 165–205

13 Lacey, M.G., Mercuri, N.B., North, R.A.: 'Dopamine acts on D2 receptors to increase potassium conductance in neurons of the rat substantia nigra zona compacta', *J. Physiol.*, 1987, **392**, pp. 397–416

14 Beckstead, M.J., Grandy, D.K., Wickman, K., *et al.*: 'Vesicular dopamine release elicits an inhibitory postsynaptic current in midbrain dopamine neurons', *Neuron*, 2004, **42**, (6), pp. 939–946

15 el Mestikawy, S., Glowinski, J., Hamon, M.: 'Presynaptic dopamine autoreceptors control tyrosine hydroxylase activation in depolarized striatal dopaminergic terminals', *J. Neurochem.*, 1986, **46**, (1), pp. 12–22

16 Marinelli, M., Cooper, D.C., Baker, L.K., *et al.*: 'Impulse activity of midbrain dopamine neurons modulates drug-seeking behavior', *Psychopharmacology (Berl.)*, 2003, **168**, (1–2), pp. 84–98

17 Yamada, S., Yokoo, H., Nishi, S.: 'Changes in sensitivity of dopamine autoreceptors in rat striatum after subchronic treatment with methamphetamine', *Eur. J. Pharmacol.*, 1991, **205**, (1), pp. 43–47

18 Sharpe, A.L., Varela, E., Bettinger, L., *et al.*: 'Methamphetamine self-administration in mice decreases GIRK channel-mediated currents in midbrain dopamine neurons', *Int. J. Neuropsychopharmacol.*, 2014, pii: pyu073, doi: 10.1093.ijnp/pyu073

19 Bello, E.P., Mateo, Y., Gelman, D.M., *et al.*: 'Cocaine supersensitivity and enhanced motivation for reward in mice lacking dopamine D2', *Nat. Neurosci.*, 2011, **14**, (8), pp. 1033–1038

20 Brooks, D.J.: 'Dopamine agonists: their role in the treatment of Parkinson's disease', *J. Neurol. Neurosurg. Psychiatry*, 2000, **68**, pp. 685–689

21 Pivonello, R., Ferone, D., de Herder, W.W., *et al.*: 'Dopamine receptor expression and function in corticotroph pituitary tumors', *J. Clin. Endocrinol. Metab.*, 2004, **89**, pp. 2452–2462

22 Scranton, R., Cincotta, A.: 'Bromocriptine-unique formulation of a dopamine agonist for the treatment of type 2 diabetes', *Expert Opin. Pharmacother.*, 2010, **11**, pp. 269–279

23 Aiken, C.B.: 'Pramipexole in psychiatry: a systematic review of the literature', *J. Clin. Psychiatry*, 2007, **68**, pp. 1230–1236

24 Beaulieu, J.-M., Gainetdinov, R.R.: 'The physiology, signaling, and pharmacology of dopamine receptors', *Pharmacol. Rev.*, 2011, **63**, pp. 182–217

25 Qi, Z., Miller, G.W., Voit, E.O.: 'Computational systems analysis of dopamine metabolism', *PLoS One*, 2008, **3**, (6), p. e2444, doi: 10.1371/journal.pone.0002444

26 Best, J.A., Nijhout, H.F., Reed, M.C.: 'Homeostatic mechanisms in dopamine synthesis and release: a mathematical model', *Theor. Biol. Med. Model.*, 2009, **6**, p. 21, doi: 10.1186/1742-4682-6-21

27 Reed, M., Nijhout, H.F., Best, J.: 'Mathematical insights into the effects of levodopa', *Front. Integr. Neurosci.*, 2012, **6**, p. 21, doi: 10.3389/fnint.2012.00021

28 Eckhoff, P., Wong-Lin, K.F., Holmes, P.: 'Optimality and robustness of a biophysical decision-making model under norepinephrine modulation', *J. Neurosci.*, 2009, **29**, pp. 4301–4311

29 Eckhoff, P., Wong-Lin, K., Holmes, P.: 'Dimension reduction and dynamics of a spiking neural network model for decision making under neuromodulation', *SIAM J. Appl. Dyn. Syst.*, 2011, **10**, pp. 148–188

30 Wang, D.H., Wong-Lin, K.: 'Comodulation of dopamine and serotonin on prefrontal cortical rhythms: a theoretical study', *Front. Integr. Neurosci*, 2013, **7**, p. 54, doi: 10.3389/fnint.2013.00054

31 Reed, M.C., Nijhout, H.F., Best, J.: 'Computational studies of the role of serotonin in the basal ganglia', *Front. Integr. Neurosci.*, 2013, **7**, p. 24, doi: 10.3389/fnint.2013.00041

32 Lo, B., Field, M.J.: 'Conflict of interest in medical research education and practice' (National Academy Press, Washington DC, 2009)

33 Ou-Yang, S.S., Lu, J.Y., Kong, X.Q., *et al.*: 'Computational drug discovery', *Acta Pharmacol. Sin.*, 2012, **33**, pp. 1131–1140

34 Kokotovic, P.V., Allenmong, J.J., Winelman, J.R., *et al.*: 'Singular perturbation and iterative separation of time scales', *Automatica*, 1980, **16**, pp. 23–33

35 Flower, G., Wong-Lin, K.: 'Reduced computational models of serotonin synthesis, release and reuptake', *IEEE Trans. Biomed. Eng.*, 2014, **61**, pp. 1054–1061

36 Veech, R.L., Eggleston, L.V., Krebs, H.A.: 'The redox state of free nicotinamide-adenine dinucleotide phosphate in the cytoplasm of rat liver', *Biochem. J.*, 1969, **115**, pp. 609–619

37 Grace, A.A., Bunney, B.S.: 'The control of firing pattern in nigral dopamine neurons: burst firing', *J. Neurosci.*, 1983, **4**, pp. 2877–2890

38 Hyland, B.I., Reynolds, J.N., Hay, J., *et al.*: 'Firing modes of midbrain dopamine cells in the freely moving rat', *Neuroscience*, 2002, **114**, pp. 475–492

39 Izhikevich, E.M.: 'Simple model of spiking neurons', *IEEE Trans. Neural Netw.*, 2003, **14**, pp. 1569–1572

40 Kita, J.M., Kile, B.M., Parker, L.E., *et al.*: 'In vivo measurement of somatodendritic release of dopamine in the ventral tegmental area', *Synapse*, 2009, **63**, pp. 951–960

41 Belle, A.M., Owesson-White, C., Herr, N.R., *et al.*: 'Controlled ionophoresis coupled with fast-scan cyclic voltammetry/electrophysiology in awake, freely moving animals', *ACS Chem. Neurosci.*, 2013, **4**, pp. 761–771

42 Benoit-Marand, M., Borrelli, E., Gonon, F.: 'Inhibition of dopamine release via presynaptic D2 receptors: time course and functional characteristics *in vivo*', *J. Neurosci.*, 2001, **21**, (23), pp. 9134–9141

43 Dreyer, J.K., Hounsgaard, J.: 'Mathematical model of dopamine autoreceptors and uptake inhibitors and their influence on tonic and phasic dopamine signaling', *J. Neurophysiol.*, 2013, **109**, pp. 171–182

44 Dreyer, J.K., Herrik, K.F., Berg, R.W., *et al.*: 'Influence of phasic and tonic dopamine release on receptor activation', *J. Neurosci.*, 2010, **30**, pp. 14273–14283

45 Einhorn, L.C., Johansen, P.A., White, F.J.: 'Electrophysiological effects of cocaine in the mesoaccumbens dopamine system: studies in the ventral tegmental area', *J. Neurosci.*, 1988, **8**, (1), pp. 100–112

46 Steinberg, E.E., Keiflin, R., Boivin, J.R., *et al.*: 'A causal link between prediction errors, dopamine neurons and learning', *Nat. Neurosci.*, **16**, pp. 966–973

47 Schultz, W.: 'Neuronal reward and decision signals: from theories to data', *Physiol. Rev.*, 2015, **95**, pp. 853–951

48 Jalewa, J., Joshi, A., McGinnity, T.M., *et al.*: 'Neural circuit interactions between the dorsal raphe nucleus and the lateral hypothalamus: an experimental and computational study', *PLoS One*, 2014, **9**, (2), p. e88003, doi: 10.1371/journal.pone.0088003

49 Wong-Lin, K., Joshi, A., Prasad, G., *et al.*: 'Network properties of a computational model of the dorsal raphe nucleus', *Neural Netw.*, 2012, **32**, pp. 15–25

50 Joshi, A., Wong-Lin, K., McGinnity, T.M., *et al.*: 'A mathematical model to explore the interdependence between the serotonin and orexin/hypocretin systems'. Proc. IEEE Engineering in Medicine and Biology Society Conf., 2011, pp. 7270–7273

51 Bjorklund, A., Dunnett, S.B.: 'Dopamine neuron systems in the brain: an update', *Trends Neurosci.*, 2007, **30**, (5), pp. 194–202

7 Appendix

7.1 Appendix 1

Analytical solutions of steady states of substrates

$$[\text{bh2}] = \left(\frac{\text{bh2}/(V_{\text{DRR}_{\text{bh2}}^k} + \text{bh2})}{1 - (\text{bh2}/(V_{\text{DRR}_{\text{bh2}}^k} + \text{bh2}))} \right) \times V_{\text{DRR}_{\text{bh2}}^k} \qquad (22)$$

$$[\text{bh4}] = \left(\frac{\text{bh4}/(V_{\text{DRR}_{\text{bh4}}^k} + \text{bh4})}{1 - (\text{bh4}/(V_{\text{DRR}_{\text{bh4}}^k} + \text{bh4}))} \right) \times V_{\text{DRR}_{\text{bh4}}^k} \qquad (23)$$

$$[\text{l} - \text{dopa}] = \frac{V_{\text{TH}}(\text{tyr, bh4, cda, eda}) \times k_{\text{AADC}, m}}{V_{\text{AADC}, \text{max}} - V_{\text{TH}}(\text{tyr, bh4, cda, eda})} \qquad (24)$$

(see (25))

7.2 Appendix 2

The following are two MATLAB codes, one (7.2.1) for simulating the full model similar to the original model in [26], and the other (7.2.2) is the reduced fast model with spiking neuronal model and autoreceptor-mediated current.

7.2.1 Full model: See Fig. 9.

7.2.2 Reduced fast model with spiking neuron and autoreceptor-mediated current: See Fig. 10.

$$[\text{cda}] = -\left(k_{\text{cda}}^{\text{Catab}} \times v_{\text{MAT}_m^k} + v_{\text{MAT, max}} - \left(V_{\text{AADC}}(\text{l} - \text{dopa}) + V_{\text{DAT}}(\text{eda}) - \left(v_{\text{MAT}_{\text{out}}^K} \times \text{vda} \right) \right) \right)$$

$$+ \frac{\sqrt{ \begin{array}{c} -\left(k_{\text{cda}}^{\text{Catab}} \times v_{\text{MAT}_m^k} + v_{\text{MAT, max}} - (V_{\text{AADC}} + V_{\text{DAT}} - (v_{\text{MAT}_{\text{out}}^K} \times \text{vda}))\right)^2 \\ -4(V_{\text{AADC}}(\text{l} - \text{dopa}) + V_{\text{DAT}}(\text{eda}) - (v_{\text{MAT}_{\text{out}}^K} \times \text{vda})) \times v_{\text{MAT}_m^k} \end{array} }}{2 \times k_{\text{cda}}^{\text{Catab}}} \qquad (25)$$

```
% Constants
dt = 0.00001; % Time steps in hours
total = 48; % Total simulated time in hours
max = ((total / dt)/2);
fire = 1; % Fire remains constant in models A-D

% Catabolism and Diffusion
kCatab_Tyr = 0.8;
kCatab_Cda = 5;
vCatab_EdaMax = 30;
kCatab_EdaM = 3;
kCatab_Hva = 3.45;
kCatab_Tyrpool = 0.2;
kRem = 400;

%Kinetic Parameters

%VAADC
vAADC_Km = 130;
vAADC_Vmax = 10000;

%VDAT
vDAT_Km = 1.4;
vDAT_Vmax= 8000;

%VDRR
vDRR_Kbh2 = 100;
vDRR_Knadph = 75;
vDRR_VfMax =150;
vDRR_Kbh4 =10;
vDRR_Knadp = 75;
vDRR_VbMax = 120;

%VMAT
vMAT_Km = 0.55;
vMAT_Vmax = 7082;
vMAT_Kout = 80;

%VTH
 vTH_Ktyr = 130;
 vTH_Kbh4 = 60;
 vTH_Vmax = 400;
 vTH_KiCda = 110;
 vTH_KiTyr = 130;

%VTYRin
vTYRin_Km = 64;
vTYRin_Vmax = 400;

%tyrTyrpool
tyrp_k1 = 6;
tyrp_km1 = 0.6;
NADPH = 124;
NADP =  0.25;
```

Fig. 9 *Full model*

```
%Declare Variables
bh2  = 41 .* ones(1,max);
bh4  = 319.* ones(1,max);
tyr   = 92.93 .* ones(1,max+1);
btyr = 97;
ldopa = 0.36.* ones(1,max);
cda  = 2.65.* ones(1,max);
vda  = 81.* ones(1,max);
eda = 0.002.* ones(1,max);
hva  = 1.* ones(1,max);
tyrpool = 1260.* ones(1,max);

vTH = 26.7 .* ones(1,max+1);
vDRR = 26.7 .* ones(1,max+1);
vTYRin = 241.* ones(1,max);
vAADC =  27.3.* ones(1,max);
vMAT = 77.5.* ones(1,max+1);
vDAT = 72.27.* ones(1,max+1);
vCatabEDA = 0.1271.* ones(1,max);

for i = 1:max

        %% Functions for calculating reaction velocities
        %%% VTH
        vTH(i) = (0.56./ (1+ (tyr(i)./vTH_KiTyr)) ) .* ((4.5 ./ ((8.*((eda(i)/0.002024).^4))+1))+0.5) .*
        ((vTH_Vmax .* tyr(i) .* bh4(i)) ./ (tyr(i).* bh4(i)+vTH_Ktyr .* bh4(i) + vTH_Ktyr .* vTH_Kbh4 .*
        (1+ (cda(i) ./ vTH_KiCda))));

        %%VDRR
        vDRR(i)  =  ((vDRR_VfMax.*bh2(i).*bh4(i))./((vDRR_Kbh2+bh2(i)).*(vDRR_Kbh4+bh4(i))))  -
        ((vDRR_VbMax .* NADPH .* NADP ) ./ ((vDRR_Knadph + NADPH) .* (vDRR_Knadp +
        NADP)));

        %%%VTYRin
        vTYRin(i) = (400 .* btyr) ./ (64 + btyr);

        %%vAADC
        vAADC(i) = (vAADC_Vmax .* ldopa(i)) ./ (vAADC_Km + ldopa(i));

        %%vMAT
        vMAT(i) = ((vMAT_Vmax .* cda(i)) ./ (vMAT_Km + cda(i))) - (vMAT_Kout .* vda(i));

        %%vDAT
        vDAT(i) = (vDAT_Vmax .* eda(i)) ./ (vDAT_Km + eda(i)) ;

        %vCatab
        vCatabEDA(i) = (vCatab_EdaMax .* eda(i)) ./ (kCatab_EdaM + eda(i)) ;

        %%Differential Equations for calculating subbstrate concentrations
        bh2(i+1) = bh2(i) + (vTH(i) - vDRR(i)) * dt;
        bh4(i+1) = bh4(i) + (vDRR(i) - vTH(i)) * dt;
        tyr(i+1) = tyr(i) + (vTYRin(i) - vTH(i) - tyrp_k1 .* tyr(i) + tyrp_km1 .* tyrpool(i) - kCatab_Tyr .*
        tyr(i)) *dt;
        ldopa(i+1) = ldopa(i) + (vTH(i) - vAADC(i)) *dt;
        cda(i+1) = cda(i) + (vAADC(i) - vMAT(i) + vDAT(i) - kCatab_Cda .* cda(i)) *dt;
        vda(i+1) = vda(i) + (vMAT(i) - fire .* vda(i)) * dt;
        eda(i+1)  = eda(i) + (fire .* vda(i) - vDAT(i) - vCatabEDA(i) - kRem .* eda(i)) *dt;
        hva(i+1) = hva(i)+  (kCatab_Cda .* cda(i) + vCatabEDA(i) - kCatab_Hva .* hva(i)) *dt;
        tyrpool(i+1)   = tyrpool(i) + (tyrp_k1 .* tyr(i) - tyrp_km1 .* tyrpool(i) - kCatab_Tyrpool .*
        tyrpool(i)) * dt;
end;
```

Fig. 9 *Continued*

```
% Constants
dt =  0.00001; % In hours. This is equivalent to dt=0.036 milliseconds
total = 0.02; % Total simulated time in hours
maxlen = (total / dt) ; % Total number of time steps in the simulation

%%%%%%%%%%%%%%%%%%%%%%%%%%%%%%%%%%%%%%%%%%%%%%%%
%%%%%%%%%%%%%%%%%%%%%%%%%%%%%%%
%%%%% Single spiking neuronal model (timescale in ms) %%%%%%%%%%%%%%%%%%%%%
%%%%%%%%%%%%%%%%%%%%%%%%%%%%%%%%%%%%%%%%%%%%%%%%%%%%%%%
%%%%%%%%%%%%%%%%%%%%%%%%%%

%---- Neuronal properties I: Parameters for recovery variable u --------
a=0.0025; % Timescale of u (~200 ms, 100-200 ms in experiments)
b=0.2; % Sensitivity of u to v (a & b: Class 1 or 2 bif; Izhikevich 2003)
c=-55; % Single spikes only
d=2; % After-spike reset of u (Izhikevich 2003)

%---- Neuronal properties II: Membrane potential v ---------------------
v=-65; % Initial values of v (at resting potential)
u=b*v; % Initial values of u
%---- Time parameters and vectorize -----------------------------------
dt_ms=0.036; % Time step of integration in ms
v_track=v.*ones(1,maxlen); % Usee to track and plot membrane potential
u_track=u.*ones(1,maxlen);

%%%%%%%%%%%%%%%%%%%%%%%%%%%%%%%%%%%%%%%%%%%%%%%%%%
%%%%%%%%%%%%%%%%%%%%%%%%%%%%
%%% Kinetic Parameters %%%
fire = ones(1,maxlen);
release = ones(1,maxlen);
vreleasefire = ones(1,maxlen);
step_change = 100000;

% Catabolism and Diffusion
kCatab_Tyr = 0.8;
kCatab_Cda = 5;
vCatab_EdaMax = 30;
kCatab_EdaM = 3;
kCatab_Hva = 3.45;
kCatab_Tyrpool = 0.2;
kRem = 400;

%Kinetic Parameters

%VAADC
vAADC_Km = 130;
vAADC_Vmax = 10000;

%VDAT
vDAT_Km = 1.4;
vDAT_Vmax= 8000;

%VDRR
vDRR_Kbh2 = 100;
vDRR_Knadph = 75;
vDRR_VfMax =150;
vDRR_Kbh4 =10;
vDRR_Knadp = 75;
vDRR_VbMax = 120;
```

Fig. 10 *Reduced fast model with spiking neuron and autoreceptor-mediated current*

```
%VMAT
vMAT_Km = 0.55;
vMAT_Vmax = 7082;
vMAT_Kout = 80;

%VTH
vTH_Ktyr = 130;
vTH_Kbh4 = 60;
vTH_Vmax = 400;
vTH_KiCda = 110;
vTH_KiTyr = 130;

%VTYRin
vTYRin_Km = 64;
vTYRin_Vmax = 400;

%tyrTyrpool
tyrp_k1 = 6;
tyrp_km1 = 0.6;
NADPH = 124;
NADP =  0.25;

%Declare Variables
bh2 = 41 .* ones(1,maxlen);
bh4 = 319.* ones(1,maxlen);
tyr = 92.93 .* ones(1,maxlen+1);
btyr = 97 .* ones(1,maxlen+1);
ldopa = 0.36.* ones(1,maxlen);
cda = 2.65.* ones(1,maxlen);
vda = 81.* ones(1,maxlen);
eda = 0.01.* ones(1,maxlen);
hva = 1.* ones(1,maxlen);
tyrpool = 1260.* ones(1,maxlen);

vTH = 26.7 .* ones(1,maxlen+1);
vDRR = 26.7 .* ones(1,maxlen+1);
vTYRin = 241.* ones(1,maxlen);
vAADC =  27.3.* ones(1,maxlen);
vMAT = 77.5.* ones(1,maxlen+1);
vDAT = 72.27.* ones(1,maxlen+1);
vCatabEDA = 0.1271.* ones(1,maxlen);
firings=[];
% Autoreceptors
f = 0.018;%
g =100;%
h = 0.05;%
I_auto = ( -f/(1+exp((-g .*(eda(1)-h))))).* ones(1,maxlen+1);

%%%%%%%%%%%%%%% Main Model Loop (Hour Timescale) %%%%%%%%%%%%%
for i = 1:maxlen

        I_auto(i) =((-f/(1+exp((-g .*(eda(i)-h)))))); %
        Inoise=0;

        J=3.8; %*(i>=(max-max/2)); % Define input current ;
```

Fig. 10 *Continued*

```matlab
thresh=0; % Spike threshold set s.t. spike amplitude ~60-70mV
fired=find(v>=thresh); % Time indices of spikes
%index of spikes
firings=[firings; i+0*fired,fired];
v(fired)=c(fired);
u(fired)=u(fired)+d(fired);
v=v+(dt_ms)*(0.04*v.^2+5*v+140-u+J+I_auto(i))+sqrt(dt_ms)*(Inoise*randn);
u=u+dt_ms*a.*(b.*v-u);% calculate recovery variable (Euler)
%update spike tracking variables
u_track(i)=u;
v_track(i)=v;

if v >= thresh
        fire(i) = fire(i) + step_change;
        %increase 'fire' variable if a spike has occured at this time point
end;


%---- functions -------
%%%% VTH
vTH(i) = (0.56 ./ (1+(tyr(i)./vTH_KiTyr))).*((4.5 ./ ((8.*((eda(i) ./
I_auto).^4))+1))+0.5).*((vTH_Vmax.*tyr(i).*bh4(i))./(tyr(i).*bh4(i) + vTH_Ktyr.*bh4(i) +
vTH_Ktyr.*vTH_Kbh4.*(1+ (cda(i)./vTH_KiCda))));
%%VDRR
vDRR(i) =
((vDRR_VfMax.*bh2(i).*NADPH)./((vDRR_Kbh2+bh2(i)).*(vDRR_Knadph+NADPH)) -
((vDRR_VbMax .* bh4(i) .* NADP ) ./ ((vDRR_Kbh4 + bh4(i)) .* (vDRR_Knadp + NADP))));
%%%VTYRin
vTYRin(i) = (400*btyr(i))./(64 + btyr(i));

%%vAADC
vAADC(i) = (vAADC_Vmax .* ldopa(i)) ./ (vAADC_Km + ldopa(i));
%%vMAT
vMAT(i) = ((vMAT_Vmax .* cda(i)) ./ (vMAT_Km + cda(i))) - (vMAT_Kout .* vda(i));
%%vDAT
vDAT(i) = (vDAT_Vmax .* eda(i)) ./ (vDAT_Km + eda(i)) ;
%vCatab
vCatabEDA(i) = (vCatab_EdaMax .* eda(i)) ./ (kCatab_EdaM + eda(i)) ;


%---- Differential equations -------------

 bh2(i) = ((bh2(i)./(vDRR_Kbh2+bh2(i)))./ (1-(bh2(i)./(vDRR_Kbh2+bh2(i))))) .* vDRR_Kbh2;
 bh4(i) = ((bh4(i)./(vDRR_Kbh4 +bh4(i)))./ (1-(bh4(i)./(vDRR_Kbh4 +bh4(i))))) .* vDRR_Kbh4;
 tyr(i+1) = tyr(i) + (vTYRin(i) - vTH(i) - tyrp_k1 .* tyr(i) + tyrp_km1 .* tyrpool(i) - kCatab_Tyr .*
 tyr(i)) *dt;
 ldopa(i) = (vTH(i) .* vAADC_Km)./(vAADC_Vmax - vTH(i));
 cda(i) = (((-(kCatab_Cda .* vMAT_Km + vMAT_Vmax - (vAADC(i) + vDAT(i) - (vMAT_Kout
 .* vda(i))))) + ...
 sqrt(((kCatab_Cda .* vMAT_Km + vMAT_Vmax - (vAADC(i) + vDAT(i) - (vMAT_Kout .*
 vda(i))))^2 - ...
 4 .* (kCatab_Cda) .* ((vAADC(i) + vDAT(i) - vMAT_Kout .* vda(i)) .* vMAT_Km)))...
 ./ (2 .* kCatab_Cda));
 vda(i+1) = vda(i) + (vMAT(i) - fire(i) .* vda(i)) * dt;
 eda(i+1)  = eda(i) + (fire(i) .* vda(i) - vDAT(i) - vCatabEDA(i) - kRem .* eda(i)) *dt;
 hva(i+1) = hva(i)+  (kCatab_Cda .* cda(i) + vCatabEDA(i) - kCatab_Hva .* hva(i)) *dt;
 tyrpool(i)  = (tyrp_k1.*tyr(i)) ./ (kCatab_Tyrpool + tyrp_km1);

end;
```

Fig. 10 *Continued*